Lattice softening and melting characteristics of granular particles

Min-Yao Zhou and Ping Sheng
Exxon Research and Engineering Co., Route 22, East Clinton Township, Annandale, New Jersey 08801
(Received 13 June 1990)

We present results of phenomenological calculations on the thermal characteristics of small granular particles. By using the self-consistent Einstein model with a Morse interaction potential, we show that as the particle size decreases, the lattice expands and the Debye temperature (as characterized by the atomic mean-square displacement) drops significantly for particle sizes below 50 Å, in good agreement with Mössbauer data on Fe particles. Variation of the melting point with particle size is calculated both by the self-consistent Einstein model, using a generalized Lindemann's criterion, and by a generalized Lennard-Jones–Devonshire (LJD) cell model. Depression of melting point by as much as 60% is obtained from the mean-field solution of the generalized LJD model for extremely small clusters. Sensitivity of the results to lattice structure has been examined. We found that the normalized melting temperature (in terms of the bulk melting temperature) is insensitive to lattice structure and exhibits a nearly universal behavior. The constraining effect of the matrix is also considered by defining a free energy, whose minimization yields the stable thermal state of small particles in the matrix environment. Mean-field LJD-model calculations using the defined free energy show that under the condition of tight coupling with the matrix the melting point of small particles may be significantly enhanced.

I. INTRODUCTION

The thermal behavior of small granular particles has been a subject of continued theoretical and experimental interest since the beginning of this century. In particular, melting temperature depression in small-particle systems has been predicted[1] and later seen experimentally[2] in a wide variety of metallic particles. Liquids trapped in porous media have also been observed to have lowered melting temperatures and very broad specific-heat peaks,[3–5] a phenomenon that has come to be known as the "melting anomaly." Related to this melting-point depression at the fundamental level is the suggestion of lattice softening in small particles. Here direct observation is rare; although indirect evidences, e.g., lattice expansion, have been seen in granular systems,[6] and the enhancement of superconducting critical temperature in granular superconductors was often attributed to lattice softening.[7]

In recent years, a combination of better measurement techniques and sample preparation, in particular the control over particle size, has enabled the experimental study of small-particle thermal behaviors to become much more quantitative. It is the intention of this work to present the results of theoretical calculations that address some of these data on the lattice softening effect[8] and the melting characteristics of small particles.[9] Since the particles in granular systems usually consist of more than a few thousand atoms, they are generally beyond the capability of numerical simulations. We are therefore limited to phenomenological calculations. By using the self-consistent Einstein model with a Morse interaction potential,[10] it is shown that the effect of lattice anharmonicity can lead to enhanced lattice expansion and softening as the particle size decreases. Both the magnitude of the resulting Debye temperature drop and its variation with particle size are in reasonable agreement with the Mössbauer data on iron.[8] However, the predicted lattice expansion is somewhat larger than the observed value. For the calculation of melting characteristics, the cell model of Lennard, Jones and Devonshire[11] (LJD) is generalized for application to small particles. Here a direct Monte Carlo evaluation of the cell model yields only a smooth transition from the solid state to the liquid state for small particles, which is expected since first-order phase transition, in its strict definition, does not occur in finite systems. However, if the mean-field transition temperature is used as indicating a "melting" temperature, then its variation versus particle size is shown to be in reasonable accord with data.[9] A separate self-consistent phonon calculation, employing a melting criterion similar to that of the Lindemann's criterion,[12] has also been carried out and is shown to yield a melting temperature versus particle size curve similar to that of the cell model. Our results are noted to agree qualitatively with those of Chui's density-functional calculations.[13]

Since in many granular systems the particles are embedded in a solid matrix, the constraining effect of the matrix on the melting behavior of the particles could be non-negligible. This is especially the case since the elastic moduli of solids are generally in the range of 10^5–10^6 atmospheres, and therefore large constraining pressure can be generated if the expansion of a small particle upon melting is not matched by the expansion of the matrix. It is shown that taking into account the effect of the constraining matrix, which is neither a constant-pressure nor a constant-value environment, requires the definition of a "free energy." By using the defined free energy in conjunction with the cell model, our calculations yield melting temperature enhancement over the free-standing par-

ticles. The melting temperature enhancement for small particles has just recently been observed.[14] However, its systematics, i.e., variation with matrix type and particle size, are still to be investigated.

In what follows, formulation of the self-consistent Einstein model for finite particles are presented in Sec. II. Numerical calculation of the mean-square displacement for small Fe particles and the comparison with Mössbauer data are given in Sec. III. This is followed in Sec. IV by the formulation and numerical evaluation of a generalized cell model for the thermal melting behavior of small granular particles. The constraining effect of the solid matrix is considered in Sec. V.

II. SELF-CONSISTENT EINSTEIN MODEL

In the present model, the atoms in a particle are assumed to interact via the Morse potential:[10]

$$v(x_{ij})=E\{\exp[-2\alpha(x_{ij}-r_0)]-2\exp[-\alpha(x_{ij}-r_0)]\} . \tag{1}$$

Here E, r_0, and α are material constants, and x_{ij} is the separation between atoms i and j:

$$x_{ij}=|\mathbf{x}_{ij}|=|\mathbf{R}_i+\mathbf{u}_i-\mathbf{R}_j-\mathbf{u}_j| \simeq|\mathbf{R}_i-\mathbf{R}_j|+\boldsymbol{\lambda}_{ij}(\mathbf{u}_i-\mathbf{u}_j) , \tag{2a}$$

$$\boldsymbol{\lambda}_{ij}=\frac{\mathbf{R}_i-\mathbf{R}_j}{|\mathbf{R}_i-\mathbf{R}_j|} , \tag{2b}$$

where $\mathbf{R}_i$ denotes the coordinate of the equilibrium position for atom i, and $\mathbf{u}_i$ denotes its displacement from that equilibrium position. The minimum of $v(x_{ij})$ occurs at $x_{ij}=r_0$ for two atoms. However, for a lattice of atoms the minimization of the sum of all the interaction potentials can result in a zero-temperature atomic separation a_0 that differs from r_0. In addition, for a finite particle the value of a_0 can vary from the center of the particle to its surface. For simplicity, in our model we will assume that (1) the atomic structure of the particle is known, and (2) a single a_0 applies to the whole particle whose value is to be obtained by minimizing the total energy of the particle at zero temperature.

At finite temperatures, the effective potential ψ_{ij} between two atoms in a particle is expected to differ from that of Eq. (1) due to the fact that $v(x_{ij})$ contains anharmonicity. ψ_{ij} may be evaluated as

$$\psi_{ij}=\langle v_{ij}\rangle=\frac{\int\prod_n d\mathbf{u}_n\, v(|\mathbf{R}_i-\mathbf{R}_j+\mathbf{u}_i-\mathbf{u}_j|)\exp\left[-\beta\sum_n \frac{1}{2}\phi_n|u_n|^2\right]}{\int\prod_n d\mathbf{u}_n\exp\left[-\beta\sum_n \frac{1}{2}\phi_n|u_n|^2\right]} , \tag{3}$$

where $\beta=1/kT$, the angular brackets denote thermal averaging as shown, ϕ_n denotes the effective force constant at atomic site n in the particle, and the index n runs over all atomic sites in the particle. Equation (3) is based on using the approximation of harmonic expansion for the local potential. By substituting Eq. (1) into Eq. (3) and using the approximation given by Eq. (2a), it is immediately seen that all integrals involving $\mathbf{u}_n$, with $n\neq i,j$, result in 1 since the numerator and denominator are the same. What remains are integrals of the type

$$\frac{\int d\mathbf{u}_i\exp(-\boldsymbol{\lambda}_{ij}\cdot\mathbf{u}_i)\exp\left[-\frac{\beta}{2}\phi_i|u_i|^2\right]}{\int d\mathbf{u}_i\exp\left[-\frac{\beta}{2}\phi_i|u_i|^2\right]}=\exp\left[\frac{1}{2\beta\phi_i}\right] ,$$

where we have used the fact $\lambda_{ij}^2=1$. Therefore,

$$\psi_{ij}=E_{ij}\{\exp[-2\alpha(R_{ij}-r_{ij})] -2\exp[-\alpha(R_{ij}-r_{ij})]\} , \tag{4a}$$

where

$$E_{ij}=E\exp\left[-\frac{\alpha^2}{\beta}(\phi_i^{-1}+\phi_j^{-1})\right] , \tag{4b}$$

$$R_{ij}=|\mathbf{R}_i-\mathbf{R}_j| , \tag{4c}$$

$$r_{ij}=r_0+\frac{3\alpha}{2\beta}(\phi_i^{-1}+\phi_j^{-1}) . \tag{4d}$$

In Eq. (4), E, α, r_0, and β are the given parameters, and ϕ_i, and R_{ij} are the unknowns to be determined self-consistently by the conditions

$$\sum_j \nabla_{R_i}\psi_{ij}=0 , \tag{5a}$$

$$\tfrac{1}{3}\sum_j \nabla_{R_i}^2\psi_{ij}=\phi_i . \tag{5b}$$

Here Eq. (5a) represents the condition of minimum energy, and Eq. (5b) is the definition of ϕ_i. (The factor $\frac{1}{3}$ represents averaging over the three directions.) In this work, we assume that the structure is known and make the approximation that

$$R_{ij}\cong R_{ij}|_{T\to 0}+\left.\frac{dR_{ij}}{dT}\right|_{T\to 0} T . \tag{6}$$

It can be shown in Appendix A that

$$\left.\frac{dR_{ij}}{dT}\right|_{T\to 0}\simeq\left.\frac{dr_{ij}}{dT}\right|_{T\to 0} . \tag{7}$$

Therefore,

$$R_{ij}\cong R_{ij}|_{T\to 0}+\frac{3\alpha}{2\beta}(\phi_i^{-1}+\phi_j^{-1}) . \tag{8}$$

By substituting Eq. (8) into Eq. (4a), we get ψ_{ij} as a function only of ϕ_i, ϕ_j, and R_{ij} ($T=0$). The zero-temperature

value of R_{ij} is determined by carrying out a one-parameter (minimum atomic separation a_0) minimization of the total interaction energy, i.e., the one-parameter solution of Eq. (5a) under the assumption of a given lattice structure. Equation (5b) then represents a set of self-consistent equations for the determination of $\{\phi_i\}$. They can be solved iteratively by Newton's method.

III. LATTICE EXPANSION AND SOFTENING

Experimental data on lattice expansion and softening have been obtained for small particles of Fe, with a body-centered-cubic (bcc) structure. To compare with data, we use a bcc lattice in the calculation with the following parameters for the Morse potential:[10]

$$r_0 = 2.8453 \text{ Å} ,$$

$$E = 0.41716 \text{ eV} ,$$

$$\alpha = 1.388\,59 \text{ Å}^{-1} .$$

These values have been obtained in prior works by fitting the various calculated results to bulk thermal properties of Fe. For simplicity, the particle shape is taken to be a cube with sides of length $2a_0 m/\sqrt{3}$, where m is the number of atoms on a side and a_0, the minimum atomic separation, is obtained by the minimization of the total energy. The variation of a_0 as a function of particle size (or diameter) D, where

$$D = 4\left[\frac{3}{4\pi}\right]^{1/3} m a_0/\sqrt{3} ,$$

is shown in Fig. 1. The maximum variation, from 2.48 to 2.59 Å, is about 4%. However, for a 20-Å particle the lattice expansion is seen to be ~2.5%. This is somewhat larger than the expansion of ~1.5% measured by x-ray[8] data. It is interesting to note that for the smallest cluster in Fig. 1 there are only three atoms across each side of the cube, or a total of 27 atoms. Even in that case the value of a_0 is still less than r_0. What this points out is the fact that the next-nearest neighbor and the next-next-nearest neighbor interactions are very important.

Lattice expansion directly leads to lattice softening. While the amount of expansion is small, yet it can have a significant effect on the potential as experienced by the atoms because the lattice parameter appears in the exponent of the Morse potential, i.e., the potential is very sensitive to changes in the lattice parameter. By following the calculational procedure as outlined in Sec. II, we obtained the $\{\phi_i\}$, for atoms in the particle. The mean-square displacement of an atom is then given by

$$\langle u_i^2 \rangle = \frac{3}{\beta \phi_i} . \tag{9}$$

Averaged over the atoms in the particle, we have

$$\overline{\langle u^2 \rangle} = 3\overline{\phi_i^{-1}} kT . \tag{10}$$

Since

$$\overline{\langle u^2 \rangle} \alpha \frac{T}{\Theta_E^2} , \tag{11a}$$

for $T > \Theta_e$, where Θ_E denotes the Einstein temperature $k\Theta_E = h\omega_0$, ω_0 being the Einstein oscillator frequency, and

$$\overline{\langle u^2 \rangle} \alpha \frac{T}{\Theta_D^2} \tag{11b}$$

for the Debye model, where Θ_D denotes the Debye temperature, we have

$$\frac{\Theta_D(D)}{\Theta_D(\infty)} = \frac{\Theta_E(D)}{\Theta_E(\infty)} . \tag{11c}$$

Therefore, a calculation on $[\overline{\langle u^2 \rangle}_\infty / \overline{\langle u^2 \rangle}_D]^{1/2}$ can directly yield $\Theta_D(D)/\Theta_D(\infty)$. The results are shown in Fig. 2 together with the Mössbauer data.[8] It is seen that the magnitude of the drop, ~30% for ~15-Å particles, is in excellent agreement with experiment. The variation of $\Theta_D(D)/\Theta_D(\infty)$ with particle size is also in reasonable

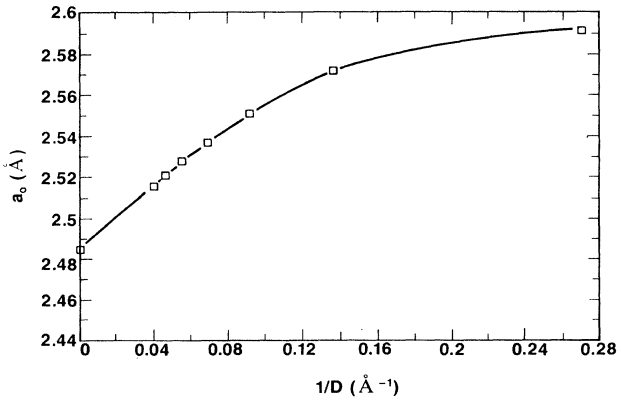

FIG. 1. Calculated zero-temperature lattice constant a_0 of Fe plotted as a function of inverse particle size. The solid line connects the calculated point, denoted by open squares.

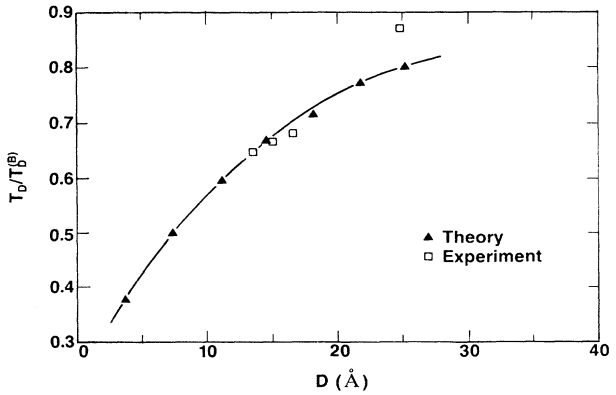

FIG. 2. Normalized Debye temperature of small Fe particles plotted as a function of particle size. The solid line connects the theoretical results calculated from the self-consistent Einstein model, denoted by solid triangles. Experimental data by Chien *et al.* (Ref. 8) are denoted by open squares.

agreement. However, the experimental data seem to indicate a more abrupt approach to the bulk value as the particle size increases than that predicted by the theory. We also note here that although in our calculation a single a_0 is used for the whole particle, yet the ϕ_i is individual to every atom of the particle. Since ϕ_i is smaller for atoms on the surface, there is thus a surface relaxation effect at finite temperatures. We expect the further relaxation of a_0 to enhance the magnitude of the Debye temperature drop.

IV. MELTING CHARACTERISTICS

Lindemann[12] has proposed a criterion for melting based on the value of $\langle u^2 \rangle$, i.e., melting occurs when $\langle u^2 \rangle$ exceeds a certain empirical value ($\sim 0.01 a_0^2$). One way to generalize such criterion for small particles is to assume that the melting of a small particle begins when the mean-square displacement of the *surface* atoms reaches the critical value. For Fe particles, a critical value of $\langle u^2 \rangle^{1/2} = 0.15$ Å is obtained by performing a separate calculation evaluating the surface mean-square atomic displacement of bulk iron at its melting temperature of 1788 K. In Fig. 3 we show the calculated variation of melting temperature as a function of inverse particle size, measured in $N^{-1/3}$ (N being the number of atoms in the particle), by using the $\langle u^2 \rangle$ criterion. For simplicity, the lattice in this case is taken to be simple cubic.

A drawback of the above approach is that it is too empirical. The correct criterion for melting transition should be the crossing of the liquid and solid free energies. Here we will generalize the phenomenological theory of Lennard-Jones and Devonshire[11] to the calculation of small-particle melting.

Consider a particle consisting of atoms arranged in a simple-cubic lattice at $T=0$. The starting point of the

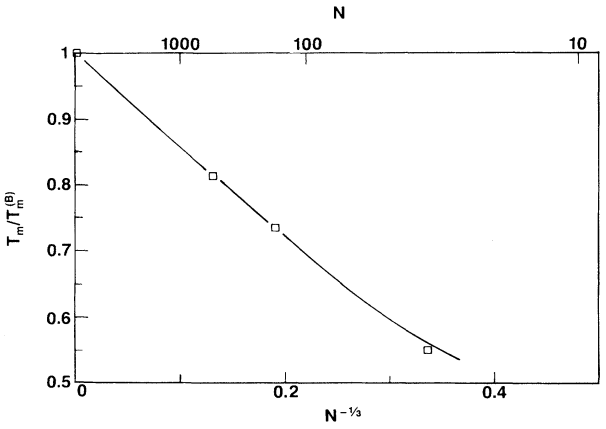

FIG. 3. Variation of the melting point as a function of $N^{-1/3}$, where N is the number of atoms in a particle. The melting temperature is calculated by using the generalized Lindemann's criterion as described in the text and the self-consistent Einstein model. Parameters used are those for Fe. However, simple-cubic-lattice structure is assumed. The solid line connects the calculated results, denoted by open squares.

LJD theory is the assumption that there are two sites, α_i and β_i, for the atom within each cell i. An order parameter S_i is defined as having value $+1$ when the atom is in site α_i and having value -1 when the atom is in site β_i. A lattice version of the LJD theory has been formulated in a prior work,[15] and the Hamiltonian of the system is given by

$$H = E_\infty - \tfrac{1}{4} \sum_{ij} W_{ij} S_i S_j \ , \tag{12a}$$

$$E_\infty = \tfrac{1}{2} \sum_{ij} (W_{ij}^{(0)} + \tfrac{1}{2} W_{ij}) \ , \tag{12b}$$

$$W_{ij}^{(0)} = (r_{ij}^{-12} - 2 r_{ij}^{-6}) W_0 \ , \tag{12c}$$

$$W_{ij} = r_{ij}^{-12} W_0 \ . \tag{12d}$$

Here the lattice constant is taken to be 1. Equation (12a) essentially tells us that when two atoms, at cells i and j and separated by r_{ij}, are both in α sites (or both in β sites) the energy is lower than that when one is in α and the other one in β. E_∞ corresponds to the energy at $T=\infty$, when there is equal chance for the occupation of α or β site in each cell, and W_{ij} [Eq. (12d)] is the extra energy incurred by one atom being at α site of cell i and another one being at β site of cell j.

The theory as applied to periodic simple-cubic lattice involves two parameters—the lattice constant a and the average order parameter $\langle S \rangle$. The value of W_0 is chosen to be 0.35 so that the bulk melting temperature $T_m^{(B)} = 1$. Our generalization of the LJD theory recognizes the fact that in absence of periodicity, each cell can have a distinct $\langle S_i \rangle$ and a_i. We make the simplifying assumption here that the nth simple-cubic shell of atoms is separated from the $(n+1)$th shell by a_n. When $a_n \neq a_{n+1} \neq a_{n=1}$ (such as at $T>0$), each cell is noted to be noncubic in shape. In the generalized model, therefore, there are as many $\langle S_i \rangle$'s as the number of atoms in a particle and a smaller number of a_n's, given by the number of shells.

The mean-field solution of the model is obtained by writing

$$S_i = \bar{S}_i + \delta S_i \ . \tag{13}$$

Here $\bar{S}_i \neq \langle S_i \rangle$, the true thermodynamic average, but may be a good approximation to $\langle S_i \rangle$. To first-order accuracy, we have

$$S_i S_j \cong \bar{S}_i \bar{S}_j + \bar{S}_j \delta S_i + \bar{S}_i \delta S_j \ .$$

The mean-field Hamiltonian is then[14]

$$H_0 = E_\infty - \sum_i V_i (S_i - \tfrac{1}{2} \bar{S}_i) \ , \tag{14a}$$

$$V_i = \tfrac{1}{2} \sum_j W_{ij} \bar{S}_j \ . \tag{14b}$$

The free energy F_0 in the mean-field approximation is given by

$$F_0 = -kT \ln \mathrm{Tr} \exp(-\beta H_0)$$
$$= E_\infty + \tfrac{1}{2} \sum_i V_i \bar{S}_i - kT \sum_i \ln[2 \cosh(\beta V_i)] \ , \tag{15}$$

At zero pressure, i.e. $p=0$ $\{\bar{S}_i\}$ and $\{a_n\}$ are determined

by the conditions

$$\frac{\partial F_0}{\partial \bar{S}_i}=0 , \tag{16a}$$

$$\frac{\partial F_0}{\partial a_n}=0 . \tag{16b}$$

Equation (16a) can be explicitly written out as

$$\bar{S}_i=\tanh(\beta V_i)=\tanh\left[\frac{\beta}{2}\sum_j W_{ij}\bar{S}_j\right] . \tag{16c}$$

Equations (16a) and (16b) constitute a set of coupled nonlinear self-consistent equations for $\{\bar{S}_i\}$ and $\{a_n\}$. When there are multiple solution sets, the physical one is chosen by the condition of minimum free energy. It should be noted that the summation over the i and j indices extends over all atoms in the particle, not just the nearest neighbors.

Mean-field equations (16a) and (16b) have been solved by using Newton's iterative method. The results were substituted into Eq. (15) to get the free energy. In Fig. 4(a), $\bar{S}=\sum_i \bar{S}_i/N$ of a particle is plotted versus temperature for the lowest free-energy solution. The corresponding lattice constant values are plotted in Fig. 4(b) for two temperatures: one below and one at the mean-field transition point. It is seen that the lattice tends to expand faster near the surface, which is an intuitive result. The abrupt jump in $\bar{S}$ is of course the result of the mean-field approximation. In reality the transition is smooth as shown below. However, if we denote the mean-field jump temperatures of $\bar{S}$ as the melting temperature T_m in a $p=0$ environment, then the variation of $T_m/T_m^{(B)}$ versus $N^{-1/3}$, where N is the number of atoms in a particle of cubic shape, is summarized in Fig. 5. It is seen that the melting point of small particles can be depressed by as much as $\sim 60\%$ from that of the bulk. Such large depression has indeed been observed in Monte Carlo simulations of small atomic clusters.[16] Also shown is the calculation using a body-centered-cubic lattice instead of the simple-cubic lattice. It is seen that the results seem to be independent of lattice structures. Comparison between Fig. 5 and Fig. 3 also indicates that, for larger particles, the amount of depression is almost the same when calculated by two radically different approaches. The difference of the two approaches only becomes manifest for smaller particles. The magnitude of the calculated melting temperature depression is also noted to be in reasonable agreement with experimental data on Bi and Sn particles.[9,17] Figures 3 and 5 therefore tell us that for not-too-small particles, there is a degree of universality to the size variation of $T_m/T_m^{(B)}$.

Since the mean-field solution is only an approximation, its accuracy has to be assessed. For this purpose we have evaluated $\langle S\rangle$ directly from the model Hamiltonian, Eq. (12a), by using the Monte Carlo method. That is,

$$\langle S\rangle=\frac{1}{N}\sum_{i=1}\frac{\int S_i\exp(-\beta H)\prod_{i,n} dS_i da_n}{\int \exp(-\beta H)\prod_{i,n} dS_i da_n} . \tag{17}$$

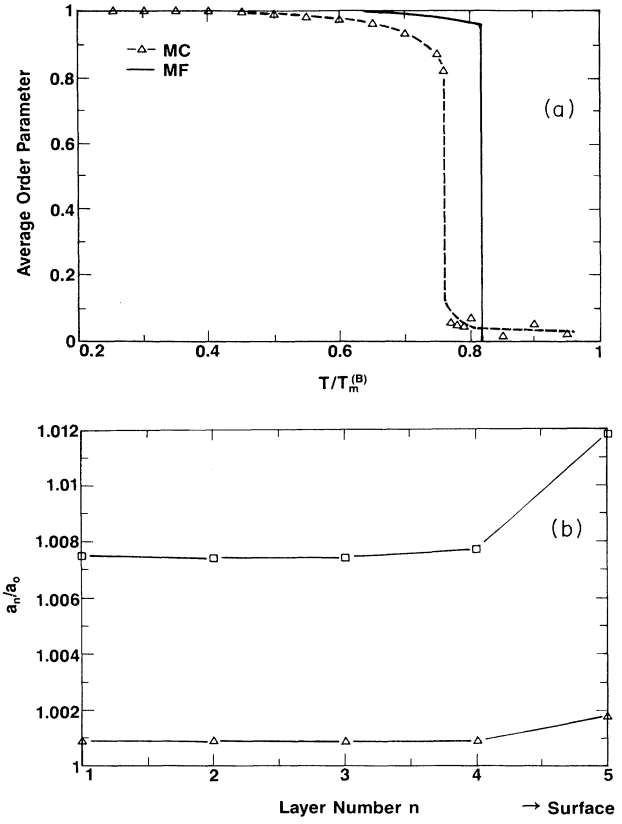

FIG. 4. (a) Comparison of the temperature dependences of mean-field $\bar{S}$ and the actual $\langle S\rangle$, evaluated by using the Monte Carlo approach. The solid line denotes $\bar{S}$. The dashed line denotes $\langle S\rangle$. Open triangles are the Monte Carlo results. The particle used in the calculation is a cube of 125 atoms with a simple-cubic lattice. For the purpose of this comparison calculation only the nearest-neighbor interactions are considered in the LJD model. The value of W_0 is set equal to 0.67 so that $T_m^{(B)}$ remains at 1. (b) Variations of the lattice constant at two different temperatures as evaluated by the mean-field theory for a $N=1000$ particle. The surface layer is seen to expand more than the interior layers as expected. The lower curve is at $T/T_m^{(B)}=0.55$. The upper curve is at the melting temperature of the particle, $T/T_m^{(B)}=0.81$.

The results are plotted as the dashed line in Fig. 4. Compared with $\bar{S}$ of the mean-field calculation, the variation of $\langle S\rangle$ is seen to be more continuous and smooth. This is the finite-size fluctuation effect as expected for any finite system. The "transition" temperature is also slightly lower than that indicated by $\bar{S}$ due to the fact that $\langle S\rangle$ is calculated with the exact Hamiltonian H and therefore contains fluctuation effects. As a function of the particle size, the ratio of the two transition temperatures is almost a constant. That means when we calculate $T_m/T_m^{(B)}$, the results are practically the same for the Monte Carlo as for the mean-field solution. The Monte Carlo evaluations therefore confirmed that the mean-field results are not too much out of line with the actual predictions of the model.

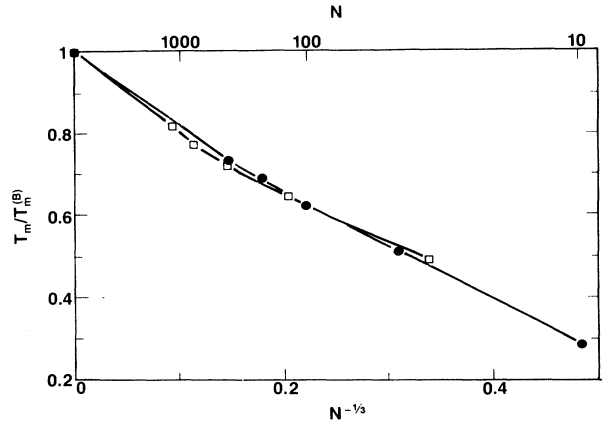

FIG. 5. Variation of the mean-field melting point as a function of $N^{-1/3}$, where N is the number of atoms in a particle. The particles used in the calculation are cubic in shape with either a simple-cubic (open squares) or a body-centered-cubic (solid circles) lattice structure. The effect of the lattice is seen to be negligible.

V. EFFECTS OF THE ELASTIC MATRIX

In the melting calculations above we have assumed that $p=0$, i.e., the particles are either free standing or decoupled from the matrix. Atmospheric pressure is neglected since it is only 10^{-5}–10^{-6} times the elastic moduli of solids (which are also in pressure units). However, if the particles are closely coupled to the matrix, then the elastic matrix would superimpose a very special environment on the resulting transition that is neither constant pressure nor constant volume.

To see how the matrix constraint would affect the melting transition, we first assume that there is a temperature at which the matrix exerts no pressure on the particle, i.e., the hole in the matrix exactly matches the particle. This temperature could be related to the formation conditions of the composite. The volume of the particle at that temperature is denoted as V_0. We assume in addition that the particle has a larger coefficient of expansion than that of the matrix. This is usually the case for metallic particles in an insulator matrix, especially near the melting point of the metal particles. Therefore the matrix would act as a pressure constraint on the particle as the temperature is raised beyond the matching point. The pressure experienced by a spherical particle may be obtained by solving a simple elastic boundary value problem as shown in Appendix B. The result is

$$p=\tfrac{2}{3}\alpha\mu\frac{\Delta V}{V_0} , \tag{18}$$

where μ is the shear modulus of the elastic matrix, $\Delta V=V-V_0$ denotes the deviation of the particle volume from V_0, and α is a dimensionless factor, given in Appendix B, that takes into account the presence of other particles in the composite. As expected, $\alpha=1$ for $\phi\rightarrow 0$, where ϕ is the volume fraction of particles. Equation (18) tells us that in the matrix environment p is a function of V, and its magnitude can be large since μ is generally large.

It should be noted here that in the present calculations the interfacial tension effect is already included (by the absence of atoms on the other side of the surface), since we have considered all the atomic interactions in the particle. However, interactions between the matrix and the particle surface atoms have not been included. In this work we have assumed that the particle surface atoms interact *incoherently* with the matrix atoms, and therefore the matrix only acts as an elastic constraint on the particle.

The second law of thermodynamics states that

$$T\,ds\geq dU+p\,dV , \tag{19}$$

where s denotes entropy and U denotes internal energy. For $p=$const and $T=$const, Eq. (19) implies

$$d(U-Ts+pV)=dG\leq 0 , \tag{20}$$

i.e., Gibb's free energy $G=U-Ts+pV$ has to minimized. However, if p is a function of V as given by Eq. (18), then the pV term has to be replaced by F_2:

$$\begin{aligned}F_2&=\int_{V_0}^{V}p(V)dV\\&=\tfrac{2}{3}\alpha\mu\int_{V_0}^{V}\frac{V-V_0}{V_0}dV\\&=-\tfrac{2}{3}\alpha\mu\left[(V-V_0)-\frac{V^2-V_0^2}{2V_0}\right] .\end{aligned} \tag{21}$$

The total new free energy Z is given by

$$Z=-kT\ln\mathrm{Tr}[\exp(-\beta H)]+F_2 . \tag{22}$$

The minimum of Z is the criterion for thermodynamic equilibrium of a small particle in the matrix environment.

Calculations based on the minimization of Z have been carried out for small particles, within the framework of the generalized LJD theory. The additional parameter μ can be nondimensionalized by expressing it in units of $kT_m^{(B)}/a_0^3$, where a_0 is the bulk lattice constant at zero temperature. V_0 is taken to be the unit-cell volume at $T=0$, calculated individually for each particle size. In Fig. 6 the melting temperature of Pb particles embedded in the MgO matrix, calculated by the mean-field LJD cell model, is plotted as a function of $N^{-1/3}$. The value of $\frac{2}{3}\mu/(kT_m^{(B)}/a_0^3)$ used is ~ 250. It is seen that compared with the $\mu=0$ case, there is considerable enhancement of T_m. For the larger particles the melting point is seen to exceed $T_m^{(B)}$. Precisely this behavior has been recently observed,[14] although in the case of the experiment the precise origin of the enhanced $T_m^{(B)}$ is still not completely clear.

In Fig. 7 we examine the effect of μ on the melting point of a sufficiently large particle so that at $\mu=0$ the melting temperature $T_m\simeq T_m^{(B)}$. As μ increases, the melting point is seen to saturate at about 1.9 $T_m^{(B)}$.

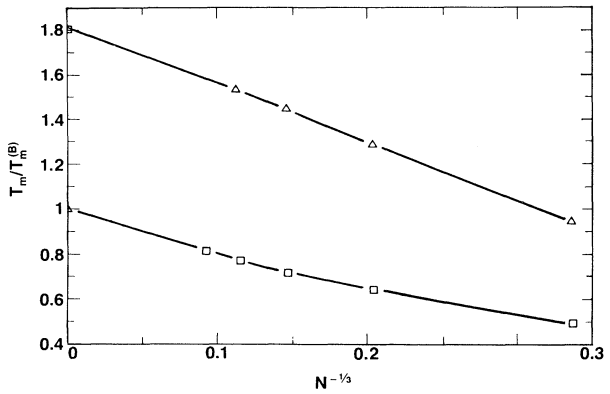

FIG. 6. Mean-field melting point variation as a function of $N^{-1/3}$, where N is the number of atoms in a particle, for particles tightly coupled to the embedding matrix. The dimensionless parameter $\frac{2}{3}\mu/(kT_m^{(B)}a_0^3)$ used is 254, suitable for Pb particles in a MgO matrix. The calculated results are denoted by open triangles. The concentration ϕ of the particles is assumed to be small so that $\alpha \simeq 1$. For comparison, the $\mu=0$ results are also plotted as open squares. Particles used in the calculations are cubic in shape with a simple-cubic-lattice structure.

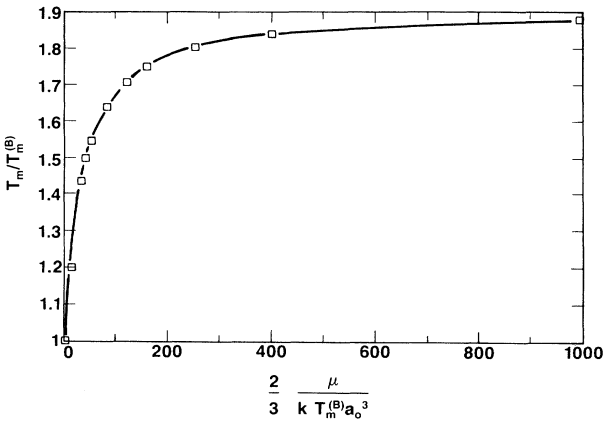

FIG. 7. Enhancement of the bulk melting point as a function of $\frac{2}{3}\mu/(kT_m^{(B)}a_0^3)$ for large particles, calculated by the mean-field solution of the LJD model. The solid line connects calculated results, denoted by open squares.

VI. CONCLUDING REMARKS

We have performed phenomenological calculations on the thermal characteristics of small particles and evaluated the effects of the constraining matrix. What emerged from these calculations are some relatively universal behaviors that include lattice expansion and softening, Debye-temperature lowering, melting-point depression, and enhancement of T_m due to matrix constraint. In particular, for the melting-point calculations the results seem to be insensitive to lattice structure and to calculational approaches. These aspects of the predictions, plus the matrix enhancement effect on the melting point, are subjects for further experimental verification.

It should be noted, however, that our calculations neglected kinetic effects. Phenomena such as supercooling, responsible for the asymmetry observed between freezing and melting, are therefore outside the realm of the present theoretical framework. Considerations on these kinetic effects in freezing and melting are presently underway. Our present formalism is also inadequate for treating the size dependence of thermal properties in materials where many-body forces are captive. An example could be gold, where the dimer separation is actually smaller than the bulk atomic separation. This presumably is due to the fact that as the number of atoms in a cluster increases, the electronic screening becomes more effective than that of the dimer. A direct manifestation of this effect is seen in the particle-size dependence of the lattice constant, which decreases as size decreases, opposite to those presented in this paper.

The authors wish to thank K. M. Unruh, S. T. Chui, J. Beamish, and C. L. Chien for many useful discussions. This work is supported by the Office of Naval Research Contract No. N00014-88-K-0003.

APPENDIX A

Here we show that in the self-consistent Einstein approximation,

$$\left.\frac{dR_{ij}}{dT}\right|_{T\to 0} \simeq \left.\frac{dr_{ij}}{dT}\right|_{T\to 0},$$

where R_{ij} is the separation of the atoms i and j in a particle, and r_{ij} is the separation that minimizes the thermal-averaged pair potential ψ_{ij}.

The value of R_{ij} is determined by Eq. (5a):

$$\sum_j \nabla_{R_i}\psi_{ij}=0\ ,$$

or

$$0=\sum_j E_{ij}\nabla_{R_i}\left\{\exp\left[-2\alpha\left[R_{ij}|_{T\to 0}+\left.\frac{dR_{ij}}{dT}\right|_{T\to 0}T-r_{ij}|_{T\to 0}-\left.\frac{dr_{ij}}{dT}\right|_{T\to 0}T\right]\right]\right.$$

$$\left.-2\exp\left[-\alpha\left[R_{ij}|_{T\to 0}+\left.\frac{dR_{ij}}{dT}\right|_{T\to 0}T-r_{ij}|_{T\to 0}-\left.\frac{dr_{ij}}{dT}\right|_{T\to 0}T\right]\right]\right\}. \tag{A1}$$

If we assume that as $T\to 0$ ($D_{ij}\to D$ as $T\to 0$) $R_{ij}|_{T\to 0}$ satisfies Eq (A1), then $dR_{ij}/dT|_{T\to 0}=dr_{ij}/dT|_{T\to 0}$ would ensure that Eq. (A1) continues to be satisfied at finite T, *provided* $E_{ij}=E\exp[-\alpha^2(\phi_i^{-1}+\phi^{-1})/\beta]$ is relatively constant, i.e., independent of i and j. This is expected to be the case because ϕ_i's represent the spring constants of interatomic interaction and vary at most by 10–20 % as T is raised. Therefore, to the same degree of accuracy we expect $dR_{ij}/dT\simeq dr_{ij}/dT$.

APPENDIX B

Consider a spherical particle of radius R_0 embedded in an elastic matrix characterized by Poisson ratio σ and Young's modulus E as shown in Fig. 8(a). The size of the hole in the matrix is assumed to fit the particle exactly. Suppose now the particle expands radially by a small amount so that the displacement in the matrix may be represented by

$$\mathbf{u}=u(r)\hat{\mathbf{e}}_r\ , \tag{B1}$$

where $\hat{\mathbf{e}}_r$ denotes the unit radial vector. That means $\nabla\times\mathbf{u}=0$, and the static elasticity equation[18] gives

$$\nabla(\nabla\cdot\mathbf{u})=0\ , \tag{B2}$$

or

$$\nabla\cdot\mathbf{u}=\text{const}\ . \tag{B3}$$

Solution of Eq. (B3) in radial coordinate yields

$$u(r)=ar+\frac{b}{r^2}\ . \tag{B4}$$

The coefficient $a=0$ because $u(r)$ has to stay finite at infinity. That means

$$b=R_0^2u_0\ , \tag{B5}$$

where $u_0=u(r=R_0)$. The pressure p on the particle surface is given by[18]

$$p=-\frac{E}{(1+\sigma)(1-2\sigma)}[(1-\sigma)u_{rr}+2\sigma u_{\theta\theta}]|_{r=R_0}\ , \tag{B6}$$

where

$$u_{rr}=\frac{du(r)}{dr}$$

and

$$u_{\theta\theta}=\frac{u(r)}{r}$$

are the radial and angular derivatives of the displacement. Combining all the factors yields

$$p=\frac{2E}{(1+\sigma)}\frac{u_0}{R_0}\simeq\frac{2}{3}\frac{E}{1+\sigma}\frac{\Delta V}{V_0}=\frac{2}{3}\mu\frac{\Delta V}{V_0}\ . \tag{B7}$$

So far we have considered only one particle in a homogeneous matrix. Suppose now there is a concentration ϕ of particles dispersed in the matrix as shown in Fig. 8(b). For the purpose of calculation, the dispersion geometry of Fig. 8(b) may be replaced by the simpler geometry of Fig. 8(c), where the effective composite shear and bulk moduli are denoted as μ' and κ', respectively. The problem to be solved now is that of a coated particle of radius R_0 and coating thickness t embedded in the effective medium. The concentration ϕ of the particles is given by $R_0^3/(R_0+t)^3$. Let the displacement in the outer (effective-medium) region be denoted as $u'(r)$. From Eq. (B4),

$$u'(r)=\frac{b'}{r^2}\ . \tag{B8}$$

Inside the coating, we have

$$u(r)=ar+\frac{b}{r^2}\ . \tag{B9}$$

Boundary condition fitting at $r=R_0+t$, i.e., $u=u'$ and $p=p'$, yields

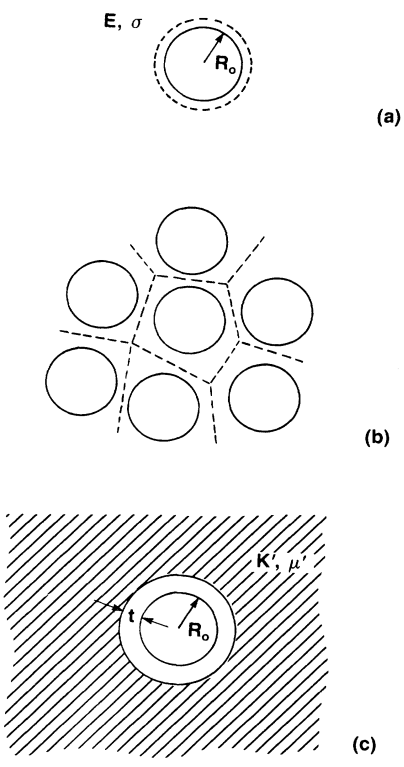

FIG. 8. (a) Schematic depiction of a particle of radius R_0 embedded in an elastic matrix with Young's modulus E and Poisson ratio σ. Expansion of the particle, shown by the dashed line, would encounter the constraining pressure of the matrix. (b) Schematic depiction of a dispersion of particles embedded in the matrix. The dashed lines segment the composite into roughly equivalent units of coated spheres. (c) For the purpose of calculating the constraining pressure, the dispersion shown in (b) is replaced by a coated particle embedded in an effective medium characterized by an effective bulk modulus κ' and an effective shear modulus μ'. The coating thickness t is determined by the condition of $R_0^3/(R_0+t)^3=\phi$.

$$0=\frac{3\kappa+2\mu'}{3\kappa'+2\mu}a+\frac{2(\mu'-\mu)}{3\kappa'+2\mu'}\frac{b}{(R_0+t)^3}\ , \tag{B10}$$

$$b=-\frac{3(\kappa-\kappa')}{2\mu'+3\kappa'}(R_0+t)^3a+\frac{2\mu+3\kappa'}{2\mu'+3\kappa'}b\ . \tag{B11}$$

From Eq. (B10) we get

$$a=-\frac{2(\mu'-\mu)}{3\kappa+2\mu'}\frac{b}{(R_0+t)^3}\ . \tag{B12}$$

Substituting Eq. (B12) into Eq. (B9) yields

$$b=\gamma R_0^2u_0\ , \tag{B13}$$

where

$$\gamma=\left[1+\frac{2(\mu-\mu')}{3\kappa+2\mu'}\phi\right]^{-1}\ . \tag{B14}$$

Comparing with Eq. (B5) shows that γ is the only additional factor in the present case. Therefore

$$p=\tfrac{2}{3}\gamma\mu\frac{\Delta V}{V_0}\ . \tag{B15}$$

The values of μ' and κ' can be calculated from the μ_m and κ_m of the particle and μ,κ of the matrix by using the effective-medium formula detailed in Ref. 19. However, the effective-medium calculation does not take into account the expansion of the embedded particles and the resulting additional hydrostatic pressure generated at a particular particle due to all the other particles. From Eqs. (B4) and (B6) it can be deduced that the pressure generated by a particle decays as r^{-3} away from its center. A straightforward summation of all such pressures at a particular site would yield divergent results. However, the presence of all the particles is expected to introduce screening, thereby making the net hydrostatic pressure p_0 finite. This additional pressure must have the form

$$p_0=C\tfrac{2}{3}\gamma\mu\frac{\Delta V}{V_0}\ , \tag{B16}$$

where C is a factor that depends on the nature of screening, the concentration ϕ, and other geometric details. Since the problem is linear, this p_0 would induce a *negative* volume change ΔV_s on each of the particles that can be superimposed on the positive ΔV. The net volume change is given by $(\Delta V)_{\rm net}=\Delta V+\Delta V_s$. By fitting the boundary condition at $r=R_0$ for $u(r)=ar$, $r<R_0$, we get

$$p_0=-\kappa_m\frac{\Delta V_s}{V_0}\ . \tag{B17}$$

Comparison with Eq. (B16) gives

$$\Delta V_s=-(\tfrac{2}{3}C\gamma\mu/\kappa_m)\Delta V\ . \tag{B18}$$

That means

$$(\Delta V)_{\rm net}=\left[1-\tfrac{2}{3}\frac{C\gamma\mu}{\kappa_m}\right]\Delta V\ . \tag{B19}$$

The total pressure $p_t=p+p_0$ can now be related to $(\Delta V)_{\rm net}$ as

$$p_t=\frac{2}{3}\frac{(1+C)\gamma}{1-\frac{2}{3}\frac{C\gamma\mu}{\kappa_m}}\mu\frac{(\Delta V)_{\rm net}}{V_0}\ , \tag{B20}$$

where we assume $2C\gamma\mu/3\kappa m\ll 1$. By dropping the subscripts t and net, we get

$$p=\tfrac{2}{3}\alpha\mu\frac{\Delta V}{V_0}\ , \tag{B21}$$

with

$$\alpha=\frac{(1+C)\gamma}{1-\frac{2}{3}\frac{C\gamma\mu}{\kappa_m}}\ . \tag{B22}$$

This is our desired result.

[1] P. Pawlow, Z. Phys. Chem. **65**, 545 (1909).

[2] M. Takagi, J. Phys. Soc. Jpn. **9**, 359 (1954).

[3] J. G. Dash, *Films on Solid Surfaces* (Academic, New York, 1975).

[4] S. C. Mraw and N. O'Rourke, Science **205**, 901 (1979).

[5] P. Sheng, R. W. Cohen, and J. R. Schrieffer, J. Phys. C **14**, L565 (1981).

[6] J. J. Hauser, Phys. Rev. B **3**, 1611 (1971).

[7] F. R. Gamble and E. J. Shimshick, Phys. Lett. **28A**, 25 (1968).

[8] J. Childress, C. L. Chien, M. Zhou, and P. Sheng (unpublished).

[9] K. M. Unruh, B. M. Patterson, and S. I. Shah (unpublished).

[10] T. Matsubara and K. Kamiya, Prog. Theor. Phys. **58**, 767 (1977). In this reference the potential for Fe is expressed in the form of $v(r)=A\exp(-ar^2)-B\exp(-br^2)$ with $A=58.86$ eV, $B=1.748$ eV, $a=0.7897$ Å, and $b=0.1508$ Å^{-2}. The parameters of the Morse potential, r_0, E, and α are obtained from v according to the condition of $\bar{v}(r_0)=v(r_0)$, $v'(r_0)=\bar{v}'(r_0)$, and $v''(r_0)=\bar{v}''(r_0)$.

[11] J. E. Lennard-Jones and A. F. Devonshire, Proc. R. Soc. London **170A**, 464 (1939).

[12] F. A. Lindemann, Z. Phys. **14**, 609 (1910).

[13] S. T. Chui (unpublished).

[14] L. Gråbaek *et al.*, Phys. Rev. Lett. **64**, 934 (1990).

[15] J. R. Schrieffer, P. Sheng, and R. W. Cohen, Phys. Scr. **35**, 212 (1987).

[16] N. Quirke and P. Sheng, Chem. Phys. Lett. **110**, 63 (1984).

[17] K. M. Unruh (private communication).

[18] L. D. Landau and E. M. Lifshitz, *Theory of Elasticity*, 2nd English Ed. (Pergamon, New York, 1970), p. 101.

[19] P. Sheng, in *Proceedings of the International Workshop on Homogenization and Effective Moduli of Composites*, edited by J. L. Ericksen, D. Kinderlehrer, R. Kohn, and J. L. Lions (Springer-Verlag, New York, 1986), p. 196.